Deformation effects on the Gamow-Teller strength distributions in the double-β decay partners ^{76}Ge and ^{76}Se

P. Sarriguren

Instituto de Estructura de la Materia, IEM-CSIC, Serrano 123, E-28006 Madrid, Spain

A theoretical approach based on a deformed quasiparticle random phase approximation built on a Skyrme self-consistent mean field is used to describe the recent measurements of the Gamow-Teller GT$^-$ strength distribution extracted from the charge-exchange reaction ^{76}Ge(^{3}He, t)^{76}As with high energy resolution. The same analysis is made to describe the Gamow-Teller GT$^+$ strength distribution measured in the ^{76}Se(d,^{2}He)^{76}As reaction. Combining these two branches, the nuclear matrix element for the two-neutrino double-β decay process is evaluated and compared to experiment. The role of the nuclear deformation on those processes is emphasized and analyzed.

I. INTRODUCTION

The Gamow-Teller (GT) nuclear response is a very fertile source of information about important issues related not only to nuclear physics [1], but also to astrophysics [2] and particle physics [3,4]. In the case of unstable nuclei this information is mainly extracted from β decays, where there is a severe restriction due to the Q-energy limitation. In the case of stable or close to stability nuclei, the GT strength is obtained from charge-exchange reactions at intermediate incident energies and forward angles [5]. Under these conditions the nuclear states are probed at small momentum transfer, and the cross section becomes proportional to the GT matrix element without the energy limitations that characterize β decays.

The spin-isospin nuclear properties in ^{76}Ge and ^{76}Se are among the most extensively studied both theoretically [6–12] and experimentally [13–18]. This is due to their significance as double-β decay partners and the implications of this process in the determination of the neutrino nature and its absolute mass [3]. The study of these nuclei is indeed a part of a large experimental program being pursued in the last several years and aimed to explore the GT properties at low excitation energies of double-β decay partners by high resolution charge-exchange reactions [1,16,19–21].

The present work is motivated by the recent high resolution charge-exchange experiment ^{76}Ge(^{3}He, t)^{76}As [14] that has allowed the unveiling of some remarkable features of this nucleus, which previous charge-exchange experiments [13] at much lower resolution were unable to identify. In particular the authors of Ref. [14] reported an unusually strong fragmentation of the GT strength that was interpreted in terms of possible effects of deformation. In Ref. [14] it was also noted a lack of correlation among the GT transition strengths feeding the same levels in ^{76}As from the two different directions, GT$^-$ measured in the ^{76}Ge(^{3}He, t)^{76}As reaction and GT$^+$ measured in the ^{76}Se(d,^{2}He)^{76}As reaction [16]. In view of this new experimental information that has become available, it is worth reconsidering the theoretical description of these nuclei and the role that deformation might play to understand the observed features.

In this work we explore the ability of the deformed proton-neutron quasiparticle random phase approximation (QRPA) approach to describe together all of this rich information available at present that includes (i) the global properties of the GT response, such as the total GT strength as well as the location and strength of the GT resonance, (ii) the GT strength distribution in the low-lying excitation region that contains much more accurate information, and (iii) the two-neutrino double-β ($2\nu\beta\beta$) decay matrix element and the implications of the single β branches in the $2\nu\beta\beta$ process.

The QRPA is one of the most reliable and broadly used microscopic approximations for calculating the correlated wave functions involved in β and double-β [22] decay processes, especially after the inclusion of particle-hole (ph) and particle-particle (pp) residual interactions. The method was first studied in Ref. [23] to describe the β strength in spherical nuclei. Subsequent extensions of the QRPA method to deal with deformed nuclei were done later in Refs. [24–29]. Deformation effects were also studied in the double-β decay process [7,9,11,30–32]. In particular, it has been found [9,30] that the nuclear matrix elements for the $2\nu\beta\beta$ process are suppressed with respect to the spherical case with a reduction factor that scales roughly with the deformation difference between parent and daughter. This suppression mechanism, which is ignored in spherical treatments may play an important role in approaching the theoretical estimates to the experiment.

As it shall be described later, our theoretical approach [28,29] is based on a deformed QRPA formalism on top of a self-consistent deformed Hartree-Fock (HF) mean field with Skyrme forces and pairing correlations in the BCS approximation. In particular, we shall study the dependence on deformation of the single β branches that build up the double-β process.

The paper is organized as follows. In Sec. II, we present a brief summary of the theoretical approach used to describe the GT properties. Section III contains the results obtained for the GT strength distributions, as well as the results for the $2\nu\beta\beta$ decay, stressing the effect of deformation. The summary and conclusions are given in Sec. IV.

II. THEORETICAL APPROACH

We describe here briefly the theoretical formalism used in this work, whose details can be found in Ref. [28,29]. First, we carry out a self-consistent deformed HF calculation with the effective nucleon-nucleon density-dependent Skyrme interaction SLy4 [33], assuming axial deformation and time reversal symmetry [34]. The single-particle wave functions are expanded in terms of the eigenstates of an axially symmetric harmonic oscillator in cylindrical coordinates using twelve major shells. Pairing correlations between like nucleons are included in the BCS approximation taking fixed pairing gap parameters for protons and neutrons, which are determined phenomenologically from the odd-even mass differences of neighboring nuclei through a symmetric five-term formula involving experimental binding energies [35]. The occupation probabilities v_i^2 of the single particle levels are computed at the end of each HF iteration and are then used to calculate the one-body density and mean field of the next iteration, so that one gets new single-particle wave functions, energies, and occupation numbers at each iteration. Therefore, the self-consistent determination of the binding energy and deformation includes pairing correlations from the beginning. After convergence, the QRPA equations are solved on the deformed ground state basis for ^{76}Ge and ^{76}Se to get their GT strength distributions and to compute the $2\nu\beta\beta$ decay matrix element.

To describe GT excitations in the QRPA, we add to the quasiparticle mean field a separable spin-isospin residual interaction in *ph* and *pp* channels. The advantage of using separable forces is that the QRPA energy eigenvalue problem is reduced to finding the roots of an algebraic equation. The *ph* part is responsible for the position and structure of the GT resonance [25,26,28]. Its coupling constant χ_{ph}^{GT} could in principle be obtained in a consistent way from the same Skyrme energy density functional as the HF mean field through the second derivatives of the energy functional with respect to the densities and averaging the contact interaction over the nuclear volume, as it was done in Ref. [28] to study exotic nuclei. The *pp* part consists of a proton-neutron pairing force and it is also introduced as a separable force [26]. The coupling constant κ_{pp}^{GT} is usually fitted to the half-lives phenomenology [26]. Following the above mentioned procedure and taking into account the experience accumulated in this mass region [36], we have chosen in this work the values $\chi_{ph}^{GT} = 0.15$ MeV and $\kappa_{pp}^{GT} = 0.03$ MeV. In addition, we will also show the sensitivity of the GT strength distributions and $2\nu\beta\beta$ nuclear matrix elements to the value of coupling constant κ_{pp}^{GT}.

The technical details to solve the QRPA equations have been described in Refs. [26,28,29]. Here we only mention that, because of the use of separable residual forces, the solutions of the QRPA equations are found by solving first a dispersion relation, which is an algebraic equation of fourth order in the excitation energy ω. Then, for each value of the energy, the GT transition amplitudes in the intrinsic frame connecting the ground state $|0\rangle$ to one phonon states in the daughter nucleus $|\omega_K\rangle$ are found to be

$$\langle \omega_K | \sigma_K t^{\pm} | 0 \rangle = \mp M_{\pm}^{\omega_K}, \qquad (1)$$

where

$$M_-^{\omega_K} = \sum_{\pi\nu} \left(q_{\pi\nu} X_{\pi\nu}^{\omega_K} + \tilde{q}_{\pi\nu} Y_{\pi\nu}^{\omega_K} \right), \qquad (2)$$

$$M_+^{\omega_K} = \sum_{\pi\nu} \left(\tilde{q}_{\pi\nu} X_{\pi\nu}^{\omega_K} + q_{\pi\nu} Y_{\pi\nu}^{\omega_K} \right), \qquad (3)$$

with

$$\tilde{q}_{\pi\nu} = u_\nu v_\pi \Sigma_K^{\nu\pi}, \quad q_{\pi\nu} = v_\nu u_\pi \Sigma_K^{\nu\pi}, \quad \Sigma_K^{\nu\pi} = \langle \nu | \sigma_K | \pi \rangle, \qquad (4)$$

in terms of the occupation amplitudes for neutrons and protons $v_{\nu,\pi}$ ($u_{\nu,\pi}^2 = 1 - v_{\nu,\pi}^2$) and the matrix elements of the spin operator connecting proton and neutron single-particle states, as they come out from the HF + BCS calculation. $X_{\pi\nu}^{\omega_K}$ and $Y_{\pi\nu}^{\omega_K}$ are the forward and backward amplitudes of the QRPA phonon operator, respectively.

Once the intrinsic amplitudes in Eq. (1) are calculated, the Gamow-Teller strength B(GT) in the laboratory frame for a transition $I_i K_i (0^+ 0) \rightarrow I_f K_f (1^+ K)$ can be obtained as

$$B_\omega(\text{GT}^\pm) = \sum_{\omega_K} [\langle \omega_{K=0} | \sigma_0 t^\pm | 0 \rangle^2 \delta(\omega_{K=0} - \omega)$$
$$+ 2 \langle \omega_{K=1} | \sigma_1 t^\pm | 0 \rangle^2 \delta(\omega_{K=1} - \omega)], \qquad (5)$$

in $[g_A^2/4\pi]$ units. To obtain this expression we have used the initial and final states in the laboratory frame expressed in terms of the intrinsic states using the Bohr and Mottelson factorization [37]. Finally, a quenching factor $g_{A,\text{eff}} = 0.7\, g_{A,\text{free}}$ is included in the calculations to take into account in an effective way all the correlations [38] that are not properly considered in the present approach.

The role of the residual interactions and BCS correlations on the GT strengths was already studied in Ref. [28,29]. The role of deformation was also studied there, where it was shown that the GT strength distributions corresponding to deformed nuclei are much more fragmented than the corresponding to spherical ones, because of the broken degeneracy of the spherical shells. It was also shown that the crossing of deformed energy levels, which depends on the magnitude of the quadrupole deformation as well as on the oblate or prolate character, may lead to sizable differences between the GT strength distributions corresponding to different shapes. These features have been exploited to use the β-decay properties as an alternative method to learn about the nuclear deformation in highly unstable isotopes [39]. It has also been shown [40] that deformation is a key ingredient to reproduce the occupation probabilities of the relevant single particle levels in the valence shells of ^{76}Ge and ^{76}Se involved in the double-β decay process that have been measured for neutrons [17] and protons [18].

The nuclear double-β decay is a rare second order weak interaction process that takes place when the transition to the intermediate nucleus is energetically forbidden or highly retarded. Two decay modes are expected, the two neutrino mode, involving the emission of two electrons and two neutrinos, and the neutrinoless mode with no neutrino leaving the nucleus. Whereas the first type is perfectly compatible with the standard model, the second one violates lepton number conservation and implies the existence of a massive Majorana neutrino. Because the nuclear wave functions and

the underlying theory for treating the neutrinoless and the two-neutrino modes are similar, the Gamow-Teller part that drives the $2\nu\beta\beta$ decay provides insight for theoretical models that are required to reproduce the available experimental information on the $2\nu\beta\beta$ half-lives.

The $2\nu\beta\beta$ decay is described in the second order perturbation of the weak interaction as two successive Gamow-Teller transitions via virtual intermediate 1^+ states. The basic expressions for the $2\nu\beta\beta$ decay within a deformed QRPA formalism can be found in [9,40]. Here we only write the half-life of the $2\nu\beta\beta$ decay

$$\left[T_{1/2}^{2\nu\beta\beta}(0_{\mathrm{gs}}^+ \to 0_{\mathrm{gs}}^+)\right]^{-1} = (g_A)^4\, G^{2\nu\beta\beta}\, \left|M_{GT}^{2\nu\beta\beta}\right|^2, \qquad (6)$$

in terms of the phase-space integral $G^{2\nu\beta\beta}$ and the nuclear matrix element $M_{GT}^{2\nu\beta\beta}$ that contains all the information of the nuclear structure involved in the process,

$$M_{GT}^{2\nu\beta\beta} = \sum_{K=0,\pm 1}\sum_{m_i,m_f}(-1)^K \frac{\langle \omega_{K,m_f}|\omega_{K,m_i}\rangle}{(\omega_K^{m_f}+\omega_K^{m_i})/2}$$
$$\times \langle 0_f|\sigma_{-K}t^-|\omega_{K,m_f}\rangle\,\langle \omega_{K,m_i}|\sigma_K t^-|0_i\rangle. \quad (7)$$

In this equation $\omega_K^{m_i}(\omega_K^{m_f})$ are the QRPA excitation energies of the intermediate 1^+ states $|\omega_{K,m_i}\rangle(|\omega_{K,m_f}\rangle)$ with respect to the initial (final) nucleus. The indices m_i, m_f label the 1^+ states of the intermediate nucleus. The overlaps are needed to take into account the nonorthogonality of the intermediate states reached from different initial $|0_i\rangle$ and final $|0_f\rangle$ ground states. Their expressions can be found in Ref. [9].

The various measurements reported for the $2\nu\beta\beta$ decay in ^{76}Ge have been analyzed in Ref. [41], where a recommended value $T_{1/2}^{2\nu\beta\beta} = (1.5 \pm 0.1) \times 10^{21}$ yr was adopted. Using the phase-space factor [9] $G^{2\nu\beta\beta}$ (^{76}Ge) $= 1.49 10^{-20}$ yr^{-1} MeV^2, we get the experimental nuclear matrix elements $M_{GT}^{2\nu\beta\beta} = 0.129$ MeV^{-1} when the bare $g_A = 1.269$ is used and $M_{GT}^{2\nu\beta\beta} = 0.216$ MeV^{-1} when quenched factors $g_A = 1$ are used.

III. RESULTS AND DISCUSSION

In this section, we first discuss the global ground-state properties of ^{76}Ge and ^{76}Se. In Table I we compare with experiment our results from microscopic SLy4 HF + BCS calculations corresponding to charge root mean square radii r_c, quadrupole moments Q_p, and quadrupole deformation parameters β. The experimental values for charge radii from Ref. [42] are well

TABLE I. Experimental and calculated charge root mean square radii r_c, intrinsic charge quadrupole moments Q_p, and quadrupole deformations β for ^{76}Ge and ^{76}Se. Experimental values for r_c are from [42]. The first experimental values for Q_p are from [43], while the second values are from [44].

		r_c (fm)	Q_p (fm^2)	β
^{76}Ge	Expt.	4.080/4.127	66(21)/164.1(2.5)	0.10/0.26
	SLy4	4.104	93.85	0.14
^{76}Se	Expt.	4.088/4.162	119(25)/205.5(2.4)	0.16/0.31
	SLy4	4.151	125.1	0.17

reproduced in our calculations. The experimental intrinsic quadrupole moments quoted correspond to values extracted from Coulomb excitation reorientation methods [43] and from electric quadrupole transition probabilities B($E2$) [44]. Our calculations produce quadrupole deformations within those experimental values.

Besides the self-consistent solution that gives us the energy minimum and the nuclear shapes at equilibrium, we are also interested in the behavior of the energy as a function of the deformation. These energy curves are obtained by performing constrained HF + BCS calculations [45], where the HF energy is minimized under the constraint of keeping the nuclear deformation fixed. The energy curves for ^{76}Ge and ^{76}Se exhibit two local minima at oblate and prolate shapes that are practically symmetric with very low energy barriers. The profiles of these curves are very shallow and roughly have the same energy for quadrupole deformations from $\beta = -0.2$ up to $\beta = 0.2$. These results are in agreement with those from similar calculations using the Gogny-D1S finite-range effective interaction [46]. Taking into account these characteristics, with oblate, spherical, and prolate shapes having practically the same energy and where small changes in the calculation can lead to different results for the absolute minimum associated to the ground state, we have opted to show here results for the GT strength distributions at various shapes corresponding to $\beta = -0.2, 0, 0.15, 0.2, 0.3$ to study the sensitivity of the GT strength distributions to the deformation.

A. Gamow-Teller strength distributions

In the upper plot of Fig. 1 we show the measured GT strength distribution as a function of the excitation energy of the daughter nucleus, extracted from the charge-exchange reactions ^{76}Ge(p, n)^{76}As [13] and ^{76}Ge(^{3}He, t)^{76}As [14]. While the former measurements were taken at a rather low resolution, the latter experiment was performed at a high energy resolution of 30 keV. The inset shows a more detailed comparison of these two measurements in the overlapping energy range below 5 MeV. The curves correspond to the same distributions obtained from a folding procedure using 1 MeV width Breit-Wigner functions, so that the original discrete spectrum is transformed into a continuous curve.

In the lower panel we can see the GT strength distributions calculated within QRPA for various deformation parameters using the same folding procedure. Taking as a reference the solid black line ($\beta = 0.15$), we can see that the main characteristics observed, such as the location and strength of the GT resonance, are qualitatively reproduced. In Table II we can see a comparison between measured and calculated GT strengths with $\beta = 0.15$ in different energy regions. In the low energy region up to 5 MeV, we have two different evaluations of the GT strength measured in Ref. [14] that compare well with the old measurements of Ref. [13]. Our calculations overestimate clearly these measurements in this range of energy. Nevertheless, if we consider the range of energy up to 7 MeV, then the calculations produce comparable results. This is also true when we compare the strength contained
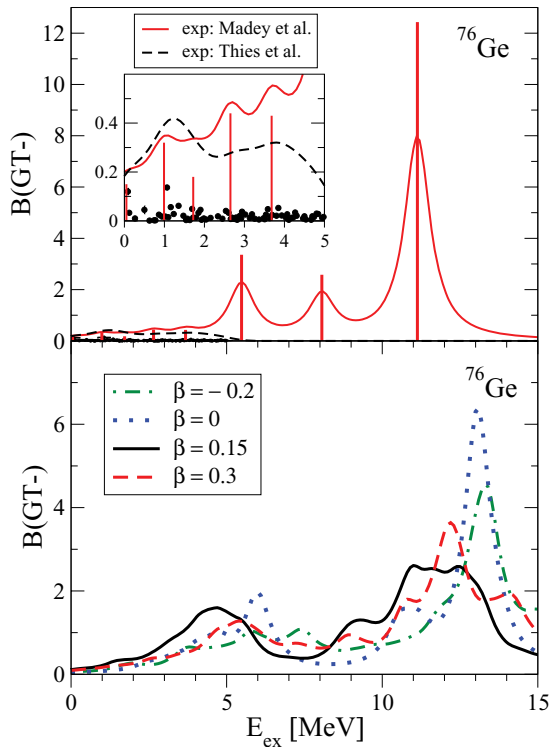
FIG. 1. (Color online) Gamow-Teller $B(GT^-)$ strength distributions in ^{76}Ge as a function of the excitation energy in the daughter nucleus. The upper panel shows the data [13,14] from different experiments. The lower panel shows calculated QRPA results with various quadrupole deformations.
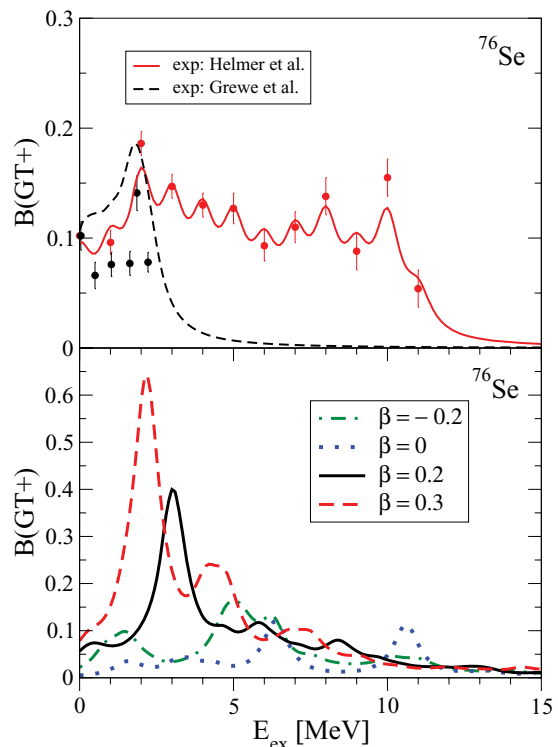

FIG. 2. (Color online) Same as in Fig. 1, but for the $B(GT^+)$ strength in ^{76}Se. Experimental data are from Refs. [15,16].

between 7 and 10 MeV, where another peak is observed, as well as when we compare the strength contained between 10 and 20 MeV, where the GT resonance is located. The total strength in the whole energy range is also well described. Calculations with other deformations produce peaks that are displaced, but qualitatively they are similar with one broad peak centered at about 5 MeV and another one centered beyond 10 MeV.

Similarly, we can see in Fig. 2 the corresponding results for the charge-exchange reactions ^{76}Se(n, p)^{76}As [15] and ^{76}Se(d,^{2}He)^{76}As [16] with an improved energy resolution of 120 keV. The curves represent again folded distributions. The lower panel shows the QRPA results for different values of quadrupole deformations. We see in this case an increased sensitivity to deformation in the low energy region where a first peak carrying most of the strength is particularly enhanced for prolate deformations. In any case, we should keep in mind that in the case of $B(GT^+)$ the total strength is much lower than in the case of $B(GT^-)$, as it must be according to the Ikeda

sum rule for $N > Z$ nuclei. Taking in this case $\beta = 0.2$ (solid black line) as a reference, we can see in Table III the strength contained in various energy ranges compared to experiment. The GT strength contained below 2 MeV is largest for the most recent data of Ref. [16]. However, as in the case of ^{76}Ge, for energies below 5 MeV both sets of data and the theoretical results are comparable. The total strength contained in the whole energy range is also well reproduced by the calculations.

This comparison tells us that the global behavior of the GT strength distribution as a whole is well reproduced in our calculations for reasonable values of the coupling constants of the residual interaction and for deformation parameters compatible with experiment.

In the next two figures, Figs. 3 and 4, we can see the comparison between the QRPA results for various deformations (blue lines) and the high resolution measurements for ^{76}Ge and ^{76}Se, respectively. In both figures we show the folded measured (solid lines) and calculated (dashed lines) distributions for a better comparison.

In the case of ^{76}Ge we can see that we get systematically less (more) strength than experimentally observed below (above) an excitation energy of about 2 MeV. This is

TABLE II. Measured and calculated GT strength in ^{76}Ge accumulated in various energy regions (MeV).

$\sum B(GT^-)$	$\sum_{0-5}$	$\sum_{0-7}$	$\sum_{7-10}$	$\sum_{10-20}$	$\sum_{0-20}$
Thies *et al.* [14]	1.60(18)/2.43(32)				
Madey *et al.* [13]	1.52	4.88	2.58	12.43	19.9
QRPA ($\beta = 0.15$)	4.0	5.5	2.2	10.6	18.3

TABLE III. Same as in Table II, but for ^{76}Se.

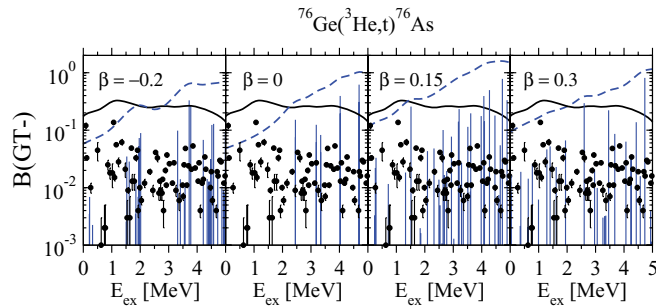| $\sum B(GT^+)$	$\sum_{0-2}$	$\sum_{0-5}$	$\sum_{5-20}$	$\sum_{0-20}$
Grewe *et al.* [16]	0.54(7)	0.7(2)	0.3(2)	1.0(4)
Helmer *et al.* [15]	0.38(3)	0.79(7)	0.64(9)	1.43(16)
QRPA ($\beta = 0.2$)	0.15	0.87	0.53	1.4

FIG. 3. (Color online) High resolution ^{76}Ge(^{3}He,t)^{76}As data [14] compared to QRPA calculations (dashed and vertical lines) with various quadrupole deformations.

true for any deformation and the total GT strength in this region is somewhat compensated. On the other hand, it is clear that the highly fragmented strength measured is only qualitatively reproduced when prolate deformations of about $\beta \sim 0.15$ are considered. In particular, the spherical strength distribution shows a concentration of the strength in a few peaks at variance with experiment. The strength distributions in Fig. 4 corresponding to ^{76}Se show also the characteristic fragmentation due to deformation that agrees better with the experiment. In this case the total calculated strength below this small range of energy is lower than experiment except for large deformations that accumulate strength around 2 MeV (see Table III).

In Figs. 5 and 6 we show the accumulated GT strength $[\sum B(\mathrm{GT})(E_{ex}) = \sum_{E<E_{ex}} B(\mathrm{GT})(E)]$ for ^{76}Ge and ^{76}Se, respectively. They are calculated from the folded distributions and correspond to QRPA calculations with various deformations using two different Skyrme forces to appreciate the sensitivity of the results to different parametrizations of the effective Skyrme interaction used. In the left panels (a) we have the results from SLy4, whereas in the right panels (b) we have the results from the Skyrme interaction SG2 [47]. The latter has been successfully tested against spin and isospin excitations in spherical [47] and deformed nuclei [28,48]. As we can see from these figures, the tendencies are very similar and the small discrepancies are only quantitative. This type of plot is very useful because it shows at the same time both the detailed structure of the strength distribution and the global behavior in terms of total strength contained at each excitation energy. In Fig. 5 the calculations for the
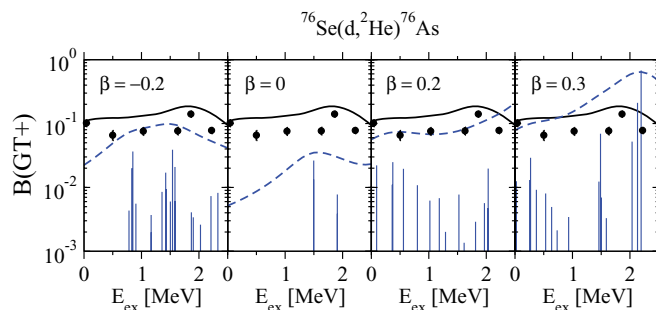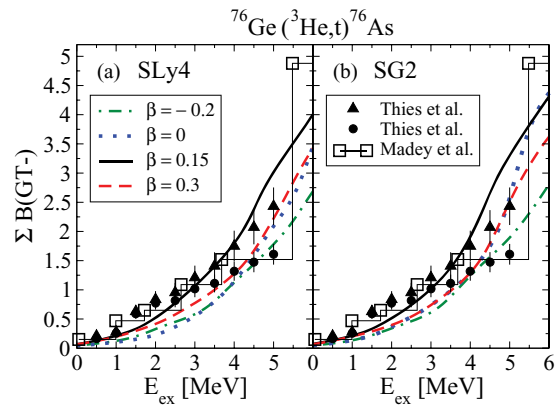

FIG. 5. (Color online) Accumulated $B(\mathrm{GT}^-)$ of ^{76}Ge as a function of the excitation energy in the daughter nucleus. The data [13,14] are compared with theoretical calculations obtained with different quadrupole deformations.

accumulated $B(\mathrm{GT}^-)$ strength in ^{76}Ge are compared to the data from ^{76}Ge(^{3}He, t)^{76}As [14] (circles) and with the data extracted over 0.5 MeV energy bins (triangles) that contain the influence of the tail of the GT resonance [14]. We also show for comparison the data from (p, n) reactions [13] (open squares). We can see that the measured strength is systematically underestimated at low excitation energy, but beyond 4 MeV the tendency is the opposite. The data are best reproduced by the calculations with a quadrupole deformation $\beta = 0.15$. In Fig. 6 we show the calculations for the $B(\mathrm{GT}^+)$ strength in ^{76}Se for various deformations. They are compared with data from the ^{76}Se(d,^{2}He)^{76}As [16] (dots) and (n, p) reactions [15] (open squares). In this case the results from spherical and oblate shapes clearly underestimate the data. Prolate deformations produce much more strength and follow better the observed trend.

Finally, it should also be mentioned that the strength of the residual proton-neutron interaction in the pp channel, κ_{pp}^{GT}, has been shown to play an important role to describe both the GT strength distributions [26,29,49] and the $2\nu\beta\beta$ nuclear matrix elements [6,9,11,30]. To demonstrate the sensitivity of the GT strength distributions to this parameter, we show
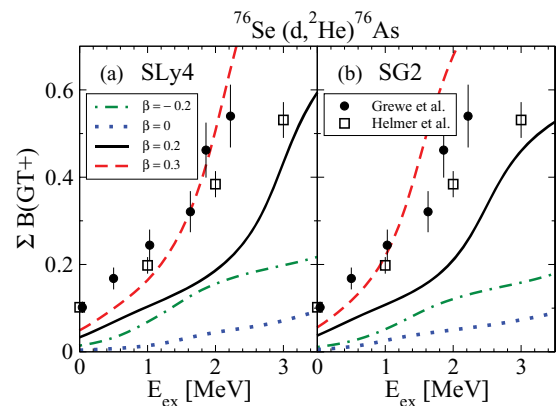

FIG. 4. (Color online) Same as in Fig. 3, but for ^{76}Se(d,^{2}He)^{76}As data [16].

FIG. 6. (Color online) Same as in Fig. 5, but for the $B(\mathrm{GT}^+)$ of ^{76}Se. Data are from Refs. [15,16].
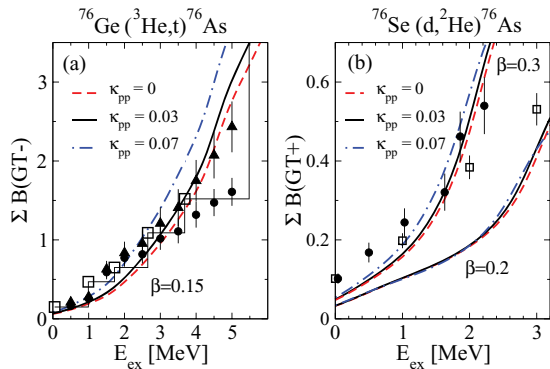
FIG. 7. (Color online) Accumulated (a) $B(GT^-)$ and (b) $B(GT^+)$ as a function of the excitation energy in the daughter nucleus. The results correspond to the Skyrme force SLy4 for various values of the coupling strength κ_{pp}^{GT} (MeV). Experimental points in (a) and (b) are as in Figs. 5 and 6, respectively.

in Fig. 7 the accumulated (a) $B(GT^-)$ and (b) $B(GT^+)$ for several values of the coupling strength κ_{pp}^{GT} (MeV). The results correspond to the Skyrme force SLy4 for various values of the deformation parameters close to the self-consistent ones and to the experiment. We observe a dispersion of the results characterized by a larger accumulation of the strength at lower energies as the value of κ_{pp}^{GT} increases. A similar tendency is found for other values of the deformation parameter. In the case of $B(GT^-)$, the spread in the profile produced by κ_{pp}^{GT} is comparable to the spread produced by the deformation [see Fig. 5(a)]. On the other hand, the effect of κ_{pp}^{GT} in the accumulated $B(GT^+)$ at low energies is much smaller than the effect produced by the deformation [see Fig. 6(a)].

B. Two-neutrino double-β decay

In this subsection we evaluate the $2\nu\beta\beta$ matrix elements for the decay of ^{76}Ge and compare them with the experimental information extracted from both the measured half-life of the process [41] and the running sum, as extracted directly from the high resolution measurements [14,16].

In Fig. 8 we can see the running sum of the $2\nu\beta\beta$ nuclear matrix element for various combinations of parent and daughter deformations as a function of the excitation energy of the intermediate nucleus ^{76}As. The shaded area indicates the experimental range for the matrix element $M_{GT}^{2\nu\beta\beta}$ extracted from the experimental half-life using bare and quenched g_A factors. Also included (red solid line) is the experimental running sum up to 5 MeV derived following the procedure explained in Ref. [14] using the GT strength distributions from [14] and [16].

The spherical description of these nuclei produce a very large matrix element that overestimates the experiment. The matrix elements are reduced when different deformations from parent and daughter are considered. In particular, the combination of deformation parameters $\beta(^{76}\text{Ge}) = 0.15$ and $\beta(^{76}\text{Se}) = 0.2$ (solid black line) produce optimal results reproducing the experiment. When the deformations are very
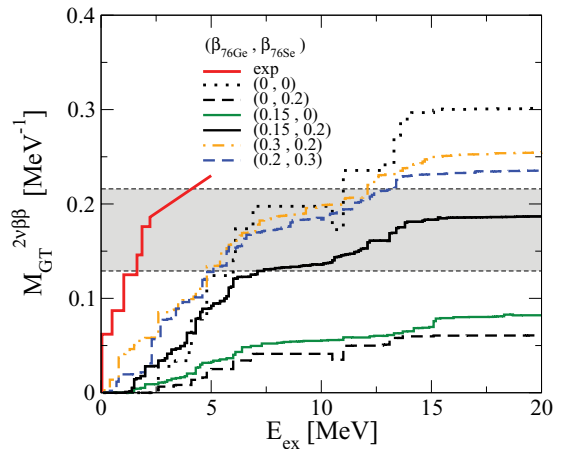

FIG. 8. (Color online) Experimental running sum [14] of the nuclear matrix element for the $2\nu\beta\beta$ decay in ^{76}Ge as a function of the intermediate excitation energy in ^{76}As, compared with results from calculations using different quadrupole deformations for parent and daughter nuclei. The shaded area indicates the experimental range extracted from the experimental half-life using bare and quenched g_A factors.

different, the matrix element becomes very small as compared to the experiment.

It should also be noted that all the calculations lie below the experimental running sum of Ref. [14] that reaches the experimental value from the half-life already at 2 MeV. As pointed out by the authors in that reference, the consequence of this is that any further contributions must be very small or must cancel each other. However, one should also take into account that the construction of the running sums in [14] was based on summing the products of GT^- and GT^+ matrix elements accumulated in different overlapping energy windows. This was done because the different resolutions of the experiments on the two branches and the lack of correlation between the GT^- and GT^+ strengths do not allow a one-to-one correspondence between the states in ^{76}As excited from ^{76}Ge and ^{76}Se. Then, this procedure provides an upper limit of
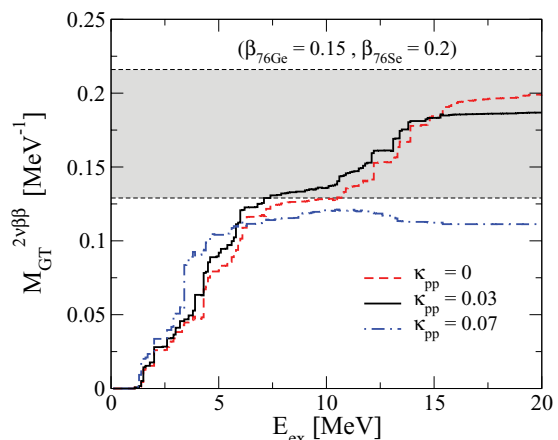

FIG. 9. (Color online) Same running sums as in Fig. 8, but for different values of the pp coupling strength. The shaded area has the same meaning as in Fig. 8.
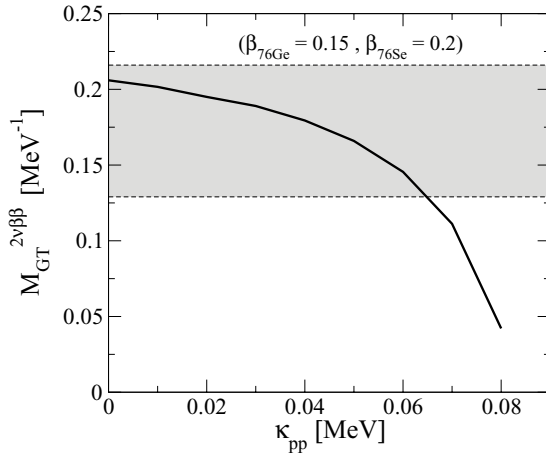
FIG. 10. Nuclear matrix element for the $2\nu\beta\beta$ decay in ^{76}Ge as a function of the coupling strength κ_{pp}^{GT}. The shaded area has the same meaning as in Fig. 8.

the actual running sum because the product of accumulated strengths is always larger than the sum of one-to-one products. In this sense, our calculations for the running sums are consistently below the experimental running sum extracted in that way.

The dependence of the running sum with the coupling strength of the proton-neutron residual interaction in the pp channel, κ_{pp}^{GT}, is shown in Fig. 9, using the deformations $\beta(^{76}\text{Ge}) = 0.15$ and $\beta(^{76}\text{Se}) = 0.20$ for the parent and daughter nuclei, respectively. The concentration of the strength at low energies produced with higher values of κ_{pp}^{GT} makes the $2\nu\beta\beta$ nuclear matrix element increase at low energies with increasing values of κ_{pp}^{GT}, but nevertheless, this increase is not enough to reproduce the experimental running sum extracted in Ref. [14]. When the running sum exhausts, the final matrix element decreases with increasing values of κ_{pp}^{GT}. This effect can be better appreciated in Fig. 10, where $M_{GT}^{2\nu\beta\beta}$ is plotted as a function of κ_{pp}^{GT}.

IV. SUMMARY AND CONCLUSIONS

In this work we have studied the GT strength distributions in the daughter nucleus ^{76}As reached from both ^{76}Ge and ^{76}Se double-β decay partners. Calculations from a deformed QRPA approach with ph and pp residual interactions based on a self-consistent Skyrme Hartree-Fock mean field with pairing

correlations are compared with data from (p, n) and (n, p) charge-exchange reactions and their associated high resolution (^{3}He, t) and $(d, ^2$He) reactions.

Using quadrupole deformations compatible with the equilibrium shapes obtained from the SLy4 interaction, which lie within the experimental values, we obtain reasonable agreement with experiment in both single-β branches, GT$^-$ in ^{76}Ge and GT$^+$ in ^{76}Se, as measured in Refs. [13,14] and [15,16], respectively, as well as with the nuclear matrix element of the $2\nu\beta\beta$ process, extracted from the experimental half-life [41]. The deformed QRPA approach used in this work is able to reproduce the gross features of the GT strength distributions, but fails to account for a detailed description of the high resolution data in the low excitation energy. Although a fine spectroscopy is beyond the scope of this HF + BCS + QRPA approach, where the use of universal effective Skyrme interactions (SLy4 in this work) intended to describe spherical and deformed nuclei all along the nuclear chart prevents reproducing accurately local details, the global performance of this approach is very reasonable. It is also worth mentioning that the agreement with experiment is optimum for the most reasonable choices of deformations and strengths of the residual interaction.

It has been shown that nuclear deformation plays a significant role in understanding the GT strength distribution, as well as in understanding the $2\nu\beta\beta$ process, where differences between parent and daughter nuclear deformations introduce a reduction factor in the nuclear matrix elements that finally determines the $2\nu\beta\beta$ half-lives.

The role of the coupling strength of the proton-neutron residual interaction in the pp channel, κ_{pp}^{GT}, to describe GT strength distributions and $2\nu\beta\beta$ nuclear matrix elements has been studied. It has been shown that, within a range of reasonable values of κ_{pp}^{GT}, its effect on the GT strength distributions at low energy is comparable or smaller than the effect produced by the deformation. It has also an effect on the $2\nu\beta\beta$ matrix elements, especially on the total matrix element that finally determines the $2\nu\beta\beta$ half-life.

[1] Y. Fujita, B. Rubio, and W. Gelletly, Prog. Part. Nucl. Phys. **66**, 549 (2011).

[2] K. Langanke and G. Martínez-Pinedo, Rev. Mod. Phys. **75**, 819 (2003).

[3] J. Suhonen and O. Civitarese, Phys. Rep. **300**, 123 (1998); A. Faessler and F. Šimkovic, J. Phys. G: Nucl. Part. Phys. **24**, 2139 (1998); H. V. Klapdor-Kleingrothaus, *Seventy Years of Double Beta Decay* (World Scientific, Singapore, 2010).

[4] J. C. Hardy and I. S. Towner, Phys. Rev. Lett. **88**, 252501 (2002); Phys. Rev. C **79**, 055502 (2009).

[5] F. Osterfelder, Rev. Mod. Phys. **64**, 491 (1992).

[6] K. Muto and H. V. Klapdor, Phys. Lett. B **201**, 420 (1988).

[7] R. Sahu, F. Simkovic, and A. Faessler, J. Phys. G: Nucl. Part. Phys. **25**, 1159 (1999).

[8] P. Sarriguren, E. Moya de Guerra, L. Pacearescu, A. Faessler, F. Šimkovic, and A. A. Raduta, Phys. Rev. C **67**, 044313 (2003).

[9] F. Šimkovic, L. Pacearescu and A. Faessler, Nucl. Phys. A **733**, 321 (2004).

[10] J. Suhonen and O. Civitarese, Phys. Lett. B **668**, 277 (2008).

[11] M. S. Yousef, V. Rodin, A. Faessler, and F. Simkovic, Phys. Rev. C **79**, 014314 (2009).

[12] O. Moreno, E. Moya de Guerra, P. Sarriguren, and A. Faessler, Phys. Rev. C **81**, 041303(R) (2010).

[13] R. Madey *et al.*, Phys. Rev. C **40**, 540 (1989).

[14] J. H. Thies *et al.*, Phys. Rev. C **86**, 014304 (2012).

[15] R. L. Helmer *et al.*, Phys. Rev. C **55**, 2802 (1997).

[16] E.-W. Grewe *et al.*, Phys. Rev. C **78**, 044301 (2008).

[17] J. P. Schiffer *et al.*, Phys. Rev. Lett. **100**, 112501 (2008).

[18] B. P. Kay *et al.*, Phys. Rev. C **79**, 021301(R) (2009).

[19] D. Frekers, Prog. Part. Nucl. Phys. **57**, 217 (2006); **64**, 281 (2010).

[20] S. Rakers *et al.*, Phys. Rev. C **70**, 054302 (2004); E. W. Grewe *et al.*, *ibid.* **76**, 054307 (2007); **77**, 064303 (2008).

[21] R. G. T. Zegers *et al.*, Phys. Rev. Lett. **99**, 202501 (2007).

[22] P. Vogel and M. R. Zirnbauer, Phys. Rev. Lett. **57**, 3148 (1986); D. Cha, Phys. Rev. C **27**, 2269 (1983); T. Tomoda and A. Faessler, Phys. Lett. B **199**, 475 (1987); K. Muto, E. Bender, and H. V. Klapdor, Z. Phys. A Hadrons Nucl. **334**, 177 (1989).

[23] J. A. Halbleib and R. A. Sorensen, Nucl. Phys. A **98**, 542 (1967).

[24] J. Krumlinde and P. Moeller, Nucl. Phys. A **417**, 419 (1984).

[25] P. Moeller and J. Randrup, Nucl. Phys. A **514**, 1 (1990).

[26] M. Hirsch, A. Staudt, K. Muto, and H. V. Klapdor-Kleingrothaus, Nucl. Phys. A **535**, 62 (1991); K. Muto, E. Bender, and H. V. Klapdor, Z. Phys. A **333**, 125 (1989); K. Muto, E. Bender, T. Oda, and H. V. Klapdor-Kleingrothaus, *ibid.* **341**, 407 (1992); H. Homma, E. Bender, M. Hirsch, K. Muto, H. V. Klapdor-Kleingrothaus, and T. Oda, Phys. Rev. C **54**, 2972 (1996).

[27] F. Frisk, I. Hamamoto, and X. Z. Zhang, Phys. Rev. C **52**, 2468 (1995); I. Hamamoto and X. Z. Zhang, Z. Phys. A **353**, 145 (1995).

[28] P. Sarriguren, E. Moya de Guerra, A. Escuderos, and A. C. Carrizo, Nucl. Phys. A **635**, 55 (1998); P. Sarriguren, E. Moya de Guerra, and A. Escuderos, *ibid.* **658**, 13 (1999); **691**, 631 (2001).

[29] P. Sarriguren, E. Moya de Guerra, and A. Escuderos, Phys. Rev. C **64**, 064306 (2001).

[30] R. Álvarez-Rodríguez, P. Sarriguren, E. Moya de Guerra, L. Pacearescu, A. Faessler, and F. Simkovic, Phys. Rev. C **70**, 064309 (2004).

[31] R. Chandra, J. Singh, P. K. Rath, P. K. Raina, and J. G. Hirsch, Eur. Phys. J. A **23**, 223 (2005).

[32] S. Singh, R. Chandra, P. K. Rath, P. K. Raina, and J. G. Hirsch, Eur. Phys. J. A **33**, 375 (2007).

[33] A. Chabanat, P. Bonche, P. Haensel, J. Meyer, and R. Schaeffer, Nucl. Phys. A **635**, 231 (1998).

[34] D. Vautherin and D. M. Brink, Phys. Rev. C **5**, 626 (1972); D Vautherin, *ibid.* **7**, 296 (1973).

[35] G. Audi, O. Bersillon, J. Blachot, and A. H. Wapstra, Nucl. Phys. A **729**, 3 (2003).

[36] P. Sarriguren, Phys. Rev. C **79**, 044315 (2009); P. Sarriguren and J. Pereira, *ibid.* **81**, 064314 (2010).

[37] A. Bohr and B. R. Mottelson, *Nuclear Structure* (Benjamin, New York, 1969 and 1975), Vols. I and II.

[38] G. F. Bertsch and I. Hamamoto, Phys. Rev. C **26**, 1323 (1982).

[39] E. Nácher *et al.*, Phys. Rev. Lett. **92**, 232501 (2004); E. Poirier *et al.*, Phys. Rev. C **69**, 034307 (2004).

[40] O. Moreno, R. Álvarez-Rodríguez, P. Sarriguren, E. Moya de Guerra, F. Simkovic, and A. Faessler, J. Phys. G: Nucl. Part. Phys. **36**, 015106 (2009).

[41] A. S. Barabash, Phys. Rev. C **81**, 035501 (2010).

[42] H. de Vries, C. W. de Jager, and C. de Vries, At. Data Nucl. Data Tables **36**, 495 (1987); G. Fricke, C. Bernhardt, K. Heilig, L. A. Schaller, L. Schellenberg, E. B. Shera, and C. W. de Jager, *ibid.* **60**, 177 (1995).

[43] N. J. Stone, At. Data Nucl. Data Tables **90**, 75 (2005).

[44] S. Raman, C. W. Nestor, Jr., and P. Tikkanen, At. Data Nucl. Data Tables **78**, 1 (2001).

[45] H. Flocard, P. Quentin, A. K. Kerman, and D. Vautherin, Nucl. Phys. A **203**, 433 (1973).

[46] www-phynu.cea.fr/science_en_ligne/carte_potentiels_microsco piques/carte_potentiel_nucleaire_eng.htm

[47] N. Van Giai and H. Sagawa, Phys. Lett. B **106**, 379 (1981).

[48] P. Sarriguren, E. Moya de Guerra, and R. Nojarov, Phys. Rev. C **54**, 690 (1996).

[49] J. Hirsch, E. Bauer, and F. Krmpotić, Nucl. Phys. A **516**, 304 (1990).